ORIGINAL ARTICLE

Enhanced durability of hot forging tools through hybrid surface treatment combining plasma nitriding with W-Ti-B and W-Ta-B nanocomposite coatings deposited using HiPIMS

T. Mościck · Pawel Widomski · M. Kaszuba · E. Wojtiuk · T. Stasiak · K. Kulikowski · R. Psiuk · M. Wiśniewska · J. Smolik

Received: 18 November 2025 / Revised: 6 May 2026 / Accepted: 9 May 2026

Abstract
The limited lifetime of hot forging tools, caused by severe wear mechanisms such as abrasion, adhesion, thermal fatigue, and plastic deformation, remains a major challenge in forging operations. The study encompasses the entire process, from concept to industrial implementation. It begins with basic laboratory tests of the innovative material, followed by the application of protective coatings on an industrial scale to forging dies, which were then successfully used in production. The research presents the development and evaluation of novel hybrid surface treatments combining plasma nitriding with nanocomposite coatings based on tungsten boride alloyed with either tantalum (W-Ta-B) or titanium (W-Ti-B). The coatings were deposited using High Power Impulse Magnetron Sputtering (HiPIMS) from SPS-fabricated ternary targets. Laboratory characterization included structural, mechanical, tribological, and oxidation resistance analyses. The W-Ti-B films exhibited superhardness above 40 GPa and superior wear resistance, while the W-Ta-B coatings demonstrated enhanced oxidation resistance and adhesion. Both coatings revealed fine columnar microstructures and favorable H/E* and H^3/E^2 ratios, indicating high resistance to plastic deformation and cracking. Industrial trials under hot forging conditions confirmed their effectiveness, with tool life extended by up to 80% compared with conventional nitrided tools. These findings demonstrate the strong potential of HiPIMS-deposited W-based boride coatings to significantly improve tool performance in demanding thermal and mechanical environments.

Keywords HiPIMS · Boride coatings · Hot forging tools · Nanocomposites · Durability

1 Introduction

Hot forging tools have a limited service life, which poses a significant economic challenge for the forging industry. The main wear mechanisms include abrasive wear, adhesive wear, thermo-mechanical fatigue, and plastic deformation, all occurring simultaneously under extreme temperature conditions [1]. Increasing demands for forging precision and process efficiency are driving the development of new solutions to improve the durability of

Published online: 01 June 2026

forging tools [2]. Current trends in forging focus on advanced tool materials and innovative surface modification technologies [3]. Protective coatings, particularly those deposited by PVD and CVD, have become the primary means of extending the lifetime of forging tools [4]. Additionally, hardfacing techniques using high-speed arc metallization and Ni-based overlays significantly enhance the tribological and corrosion resistance of tool steels, offering cost-effective alternatives to traditional coatings [5]. Hybrid layers that combine plasma nitriding with such coatings are particularly popular. Coatings used in forging must provide high hardness at elevated temperatures, good thermal stability, and resistance to both abrasive and adhesive wear. Equally important is coating elasticity, which prevents cracking under cyclic thermo-mechanical stresses. Recent research has focused on coatings modified with refractory metals, which show enhanced thermal stability. The development of nanotechnology is creating new opportunities for coatings with superior tribological and thermal properties [6].

To further increase tool durability, various approaches are employed, including mechanical surface treatments (e.g., ball burnishing), thermo-chemical hardening of surface and subsurface layers (carburizing, nitriding, nitrocarburizing) [7], welding-based methods for applying thick functional layers (cladding, hardfacing), and coatings with varying thicknesses, properties, and deposition methods [8].

Among the deposition methods used to enhance durability, PVD and CVD are the most frequently applied. CVD enables the deposition of very thin and hard coatings. The first attempts to coat tool steels with CVD layers were made in the 1980 s; however, because the process temperature exceeded 1000 °C, these coatings were not applied in forging at that time [9]. Today, with plasma assistance or process activation (PE/PACVD), the treatment can be carried out at lower temperatures, enabling its use on heat-treated steels. The first CVD applications on forging tools involved nitrided layers combined with superhard (55 GPa) TiBN coatings consisting of TiN, TiB, and TiB2, which extended the service life of dies and punches in warm and hot forging processes [10]. Comparable studies on hot forging tools confirmed the effectiveness of TiCN and TiN–TiB2 coatings in extending tool life and reducing friction. Likewise, multilayer coatings such as TiN–TiCN–TiC, along with those mentioned above, were successfully applied in precision forging [11]. The CVD process also allows the formation of multilayer and gradient coatings [12], which reduce both adhesive and abrasive wear [13].

In PVD technologies, the first coatings applied were titanium and chromium nitrides, which showed good performance on cutting tools [14]. Later, coatings containing aluminum and titanium compounds showed potential for application on hot forging tools [15]. Titanium and aluminum nitrides improve oxidation resistance at high temperatures and increase hardness. Some of the earliest application studies described hybrid layers combining nitriding with TiN, CrN, (Ti, Cr)N, and Ti(C, N) coatings [16]. Further applications emerged, including Oerlikon Balzers coatings (Balinit – TiN/TiAlN), where hybrid layers on forging dies resulted in several-fold improvements in durability [17]. Likewise, tool life in forging processes increased by at least 100% with the use of CrN and TiN coatings [18]. Initial tests indicated that tools with hybrid layers exhibited different wear mechanisms. Valuable results on CrN- and ZrN-based coatings, studied for fatigue cracking resistance and oxidation, were reported in [19]. Subsequent studies examined die durability during the first several hundred forging cycles [20].

PVD processes allow the deposition of coatings with diverse chemical compositions, offering significant potential for producing layers with tailored properties, as well as gradient and multilayer structures [21]. Examples of improved tool life in forging processes are reported in [22], which also provided a valuable discussion of damage mechanisms, highlighting the reduced contribution of friction to overall wear. Similarly, in [23], surface changes in tools with a nitrided layer and a (Ti0.375Al0.625)N/γ-Al2O3 coating after 1000 forging cycles were analyzed. Another example is a 76% reduction in die wear achieved with a nanocomposite TiAlN (nc-TiAlN) coating [24]. Likewise, CrVN coatings with 13% vanadium have demonstrated good wear resistance in forging processes. Further applications involved multi-material coatings such as CrTiAlN [25], TiCrAlN, TiAlintermetallic/AlCrTiN, Cr3C2–Cr/Ni, (AlN–CrN–TiN)multinano, Ti/TiN/TiAlNgradient/(TiAlN/VN)multinano, Ti/(TiN–ZrN)multinano/TiN, Ti–W–Al–Cr multilayer, and others [26]. Recent results also point to the use of AlCrSiN [27] coatings and TiAlN coatings with TiB2additions [28].

An important group of coatings comprises doped titanium nitride coatings deposited by magnetron techniques [29, 30], which, in addition to their resistance to elevated temperatures, exhibit a highly favorable hardness-to-stiffness (Young's modulus) ratio, thereby providing enhanced resistance to cracking. In recent years, coatings based on transition metal borides have also been the subject of similar investigations [31, 32]. Materials such as TiB2, ZrB2, Table 2 and WB2 are characterized by high melting points, high thermal conductivity, and very high hardness [33]. The W1-xTaxB2-y [34] and W1-xTixB2-y [35] films deposited by magnetron techniques have been found to be superhard (H > 40 GPa) while remaining relatively flexible (E < 400 GPa). Combined with the low residual stresses in the layer, these properties place them within the class of modern single-layer nanocomposite coatings [36]. Depending on the alloying element, WB_2 can achieve high oxidation resistance (e.g., Ta, Al) [34, 37] or superior abrasion resistance (e.g., Ti) [35]. These properties primarily arise from the hexagonal crystal structure of these compounds, which provides very strong covalent bonding between boron atoms while also enabling the formation of solid solutions with other transition metals. Vacancies in the crystal lattice are also significant, as they not only improve mechanical properties [38] but also stabilize the metastable α-WB_2 structure [39]. Moreover, magnetron deposition methods make it possible to obtain a fine-grained structure, introducing additional strengthening mechanisms [40]. A further advantage of WB_2 or TaB_2 borides is the presence of high atomic weight metals (mW = 183.8 amu, mTa = 180.9 amu), which, in the case of deposition by high-power impulse magnetron sputtering (HiPIMS), enables the fabrication of fully dense films [41]. The increase in surface temperature due to bombardment by heavy metal ions allows for a significant reduction in the deposition temperature, which is usually achieved by external heating. Recent studies have shown that it is possible to obtain excellent properties of boride coatings without the need for external heating [31]. In this case, the ionization of the sputtered material is ensured by high-power pulses, and the ions are directed toward the substrate through appropriate polarization. Films produced in this way are highly densified, exhibit lower residual stresses, and demonstrate improved adhesion to the substrate [29]. A disadvantage of the method is its relatively low deposition rate, often necessitating the combined use of DCMS and HiPIMS. However, research by Psiuk et al. [42] has shown that it is possible to increase the deposition rate in HiPIMS while simultaneously reducing the substrate temperature. The W1-xTaxB2-y [42] and W1-xTixB2-y [35] films deposited using HiPIMS from single ternary targets at temperatures above 300 °C exhibit high resistance to elevated temperatures (up to 1000 °C in vacuum in the case of Ta alloying) and very high resistance to abrasive wear ($WR = 2.1 \times 10^{-7}$ mm³/Nm for Ti doping).

Reducing the deposition temperature and limiting the number of sources allow the method to be transferred from laboratory to industrial scale. For more complex tool geometries, the number of ternary target sources can be increased during deposition.

The aim of this study is to develop protective coatings with suitable mechanical and thermal properties to enhance tool durability under service conditions. This work presents the technological process, from laboratory research to coating deposition on tools. The concept was validated during tool operation under production conditions. After industrial production testing, the tools were subjected to wear analysis, and the results were compared with those obtained from tools that were only nitrided. Because forging tools must operate at high temperatures while maintaining abrasion resistance under high loads, the study also aims to compare two additives incorporated into tungsten diboride coatings. Alloying with titanium provides improved wear resistance, while the addition of tantalum provides the W-B layers with greater resistance to high temperatures. A comparison conducted under production conditions will assess the suitability of both solutions.

2 Methodology

2.1 Preliminary studies

The first stage of the research involved activities carried out on samples to determine the physical, chemical, and mechanical properties of the developed coatings. In this stage, a target was prepared using the SPS method, the

coatings were deposited by magnetron sputtering, and subsequently, the properties of the coatings were thoroughly analyzed under laboratory conditions.

2.1.1 Film deposition

In the preliminary studies, based on previous work [35, 42, 43], films deposited from spark plasma sintered (SPS) targets with a 2-inch diameter and compositions of $W_{0.76}Ta_{0.24}B_{2.5}$ or $W_{0.76}Ti_{0.24}B_{2.5}$ were selected as candidates for protective tool coatings. Further details on the sintering process are provided in [44]. Prior to deposition, the target discs were ground and plasma etched for 15 min. Deposition was carried out using a 2-inch TORUS® magnetron cathode operating in HiPIMS mode. The deposition parameters were: pulse length $\tau = 20$ µs, frequency $f = 1000$ Hz, peak power Pmax = 300 W, and substrate bias voltage $U = -50$ V (DC). The target-to-substrate distance was set to $s = 8$ cm, with the target positioned directly opposite the substrate. To ensure process purity, the vacuum chamber was evacuated to 5×10^{-5} Pa and then backfilled with argon to 0.6 Pa (argon flow during deposition: 10–11 sccm). The 1-inch diameter substrates were made of QRO-90 tool steel. Before deposition, the substrates were glow-discharge nitrided and then polished. They were subsequently cleaned in acetone and isopropyl alcohol using an ultrasonic bath, and additionally subjected to plasma etching (bias DC − 700 V) for 15 min. The W–Ta–B coatings were deposited at 450 °C and the W–Ti–B coatings at 350 °C, each deposited for 90 min. The deposition temperatures were optimized separately for both coating composition based on preliminary laboratory studies to achieve the optimal mechanical properties and deposition rate.

2.1.2 Analysis

Due to surface roughness, the films were analyzed with a VK-X100 laser confocal microscope (Keyence, Mechelen, Belgium). The measurements were conducted according to ISO 4288. Five profiles were measured on each tested surface, and the arithmetic mean roughness value (*Ra*) was determined. Sample preparation for TEM analysis was carried out by focused ion beam (FIB) milling using a SEM (ThermoFisher Scientific™ Helios™ 5 UX, USA). After cutting lamellas, STEM imaging was performed at 15 kV acceleration voltage to reveal the microstructure and coating thickness. TEM bright field images were acquired using a Jeol JEM-F200 TEM (Jeol, Japan) at 200 kV acceleration voltage. Selected area electron diffraction (SAED) in TEM was used to obtain crystallographic data. The surface morphology and chemical composition of the oxide layer were examined with SEM+EDS (SM6010PLUS/LV, JEOL, Japan). To avoid substrate influence, X-ray diffraction (XRD) measurements (Bruker D8 Discover diffractometer with filtered Cu Kα radiation, $\lambda = 0.154056$ nm) were performed in 2θ scan mode with a fixed incidence angle of 8°.

Because of the limited accuracy of SEM-EDS for light elements such as boron, the TOF-ERDA method was employed to determine elemental composition. Recoils were generated using a 23 MeV $^{127}I^{7+}$ ion beam with an incidence angle of 20° on the sample surface. The TOF-ERDA spectrometer was positioned at an angle of 37.5° relative to the beam direction. Due to the resolution limits in distinguishing metals with similar atomic masses (e.g., tungsten and tantalum), the films were additionally investigated using energy-dispersive X-ray spectroscopy (EDS).

Nanoindentation was performed with a NanoTest Vantage system (Micro Materials, Wrexham, United Kingdom). A Berkovich-type indenter was loaded and unloaded at 1 mN/s up to a peak load of 20 mN, which was held for 2 s. At least 15 valid indents were made on each coating. The indentation depth was kept below 10% of the film thickness. Hardness was determined from the peak load and the projected contact area, while the reduced Young's modulus was calculated using the Oliver–Pharr method [44]. Since Young's modulus is more sensitive to substrate influence, its values were determined based on extrapolation to low loads [43].

To investigate the effect of elevated temperature on coating quality, samples were heated at 400, 550, and 700 °C in air in a Czylok PRC1800 metallurgical tube furnace. Samples were held at the target temperature for 1 h and subsequently analyzed by SEM, XRD, and EDS to assess surface morphology and oxidation products.

Film adhesion and critical load tests were performed using a CSM scratch-test device. The procedure involved scratching the sample surface with an indenter of known blade geometry. The sample was moved at a constant speed perpendicular to the blade, which was pressed against the surface under a controlled normal load, thereby penetrating the material. During the test, the normal load, friction force, penetration depth, and the acoustic emission signal associated with cracking and layer decohesion were continuously recorded. The tests were conducted with the following parameters: scratch length of 8 mm, linearly increasing load from 1 to 20 N, using a Rockwell diamond indenter with a tip radius of 0.2 mm. Adhesion evaluation of the tested coatings was based on the correlation of the recorded parameters (load, friction force, penetration depth) with microscopic examination of the scratches performed using a Nikon Eclipse LV150N optical microscope.

Wear resistance tests were carried out using the ball-on-disc method with a T-21 tribotester (ITEE, Radom, Poland), in accordance with ASTM G99-05. Measurements were performed at room temperature (22 ± 3 °C) without the use of external lubricants. The counterbodies were polished Al_2O_3 ceramic balls with a diameter of 6.35 mm (grade G28). Tests were conducted at a sliding speed of 0.05 m/s under a load of 2 N, with a wear track radius of 3 mm. Each test was performed with a fixed number of 1000 revolutions, corresponding to a sliding distance of 18.85 m. Prior to testing, the surfaces of both the sample and the counterbody were cleaned with acetone to remove contaminants.

2.2 Industrial trials

In this part, forging tools used in hot forging processes were prepared, for which a hybrid process of nitriding and coating deposition was carried out. The tools were then subjected to service tests under laboratory and industrial conditions, followed by an analysis of their wear.

2.2.1 Layer preparation – hybrid surface treatment of forging dies

Hybrid surface treatment of forging dies was carried out in two material variants:

- Variant 1: plasma nitriding layer + $W_{0.76}Ta_{0.24}B_{2.5}$ – coating.
- Variant 2: plasma nitriding layer + $W_{0.76}Ti_{0.24}B_{2.5}$ - coating.

The treatment was performed using a multi-step hybrid approach, in which individual surface engineering processes were carried out separately, i.e., plasma nitriding and magnetron sputtering. Between successive stages of surface treatment, the dies underwent mechanical surface processing (shot blasting and polishing) to remove all contaminants and traces of iron nitrides formed on the die surface during the nitriding process. The scheme of the hybrid surface treatment is shown in Fig. 1.

Prior to the nitriding process, the components were subjected to chemical cleaning using the cleaning agent iBiotec Neutralena 2015 under the following parameters:

- Medium: iBiotec Neutralena 2015,
- Time: t=30 min,
- Temperature: T=40 °C,
- Cleaning unit: Polsonic.

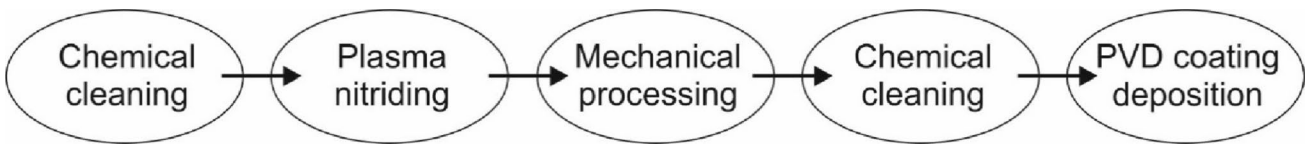

Fig. 1 Schematic of the hybrid surface treatment applied to the investigated forging dies

Table 1 Parameters of the glow-discharge plasma nitriding process

Process stage	Temperature T [°C]	Pressure p [mbar]	Atmosphere N_2/(N_2+H_2) [%]	Gas flow $q_{N2/H2}$ [sccm]	Time t [h]
Heating	↑to 520	3.5	12.1	100/400	-
1	520	4.3	8.1	130/1458	1.5
2			7.6	120/1471	1.5
3			6.8	110/1487	4.0
Cooling	↓below 150	$4.3 \rightarrow 2 \times 10^{-5}$	-	-	-

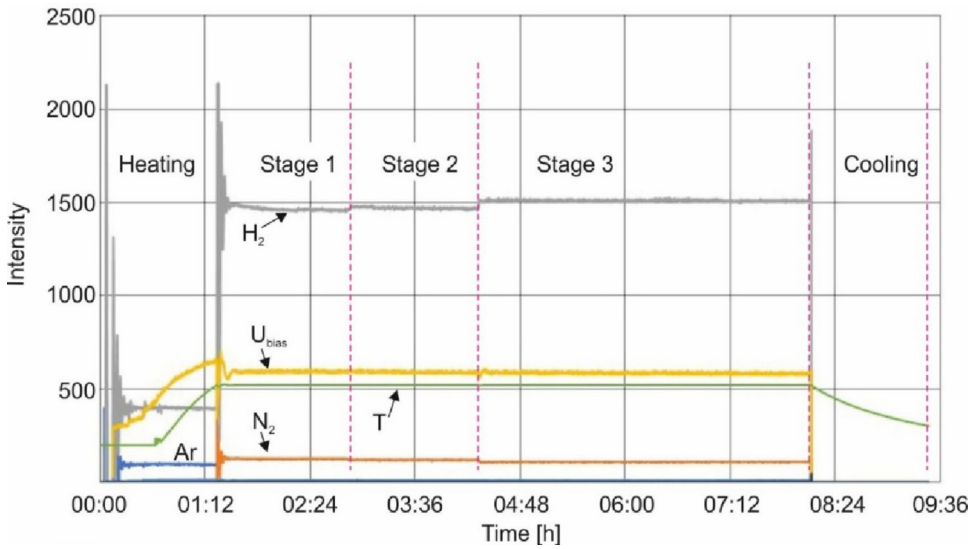

Fig. 2 Record of process parameter changes during glow-discharge nitriding

Glow-discharge plasma nitriding was carried out in a stepwise nitriding cycle in an N_2+H_2 atmosphere with a variable N_2/(N_2+H_2) ratio. For this purpose, a PVD-Standard unit equipped with an N_2+H_2 process atmosphere composition control system was used. The parameters of the glow-discharge plasma nitriding process are presented in Table 1. The obtained thickness of the nitrided diffusion layer for the applied parameters was 90 µm, and the maximum hardness of the nitrided layer was 1100 HV0.1.

During nitriding, the component temperature was monitored online using a pyrometer. Changes in nitriding parameters over time are shown in Fig. 2.

Mechanical surface treatment was performed in two stages:

Stage 1 – shot blasting: abrasive – fused alumina type 99 A (200–300 µm);

pressure: p_{GLAS} = 4 bar;

nozzle diameter: d = 8 mm.

Stage 2 – polishing: abrasive – polishing fleece 360; polishing fleece 1500.

After mechanical treatment, immediately before PVD deposition, the components were again chemically cleaned with iBiotec Neutralena 2015, using the same parameters as previously applied.

The selected PVD coatings, W–Ta–B and W–Ti–B, were deposited using High Power Impulse Magnetron Sputtering (HiPIMS). For this purpose, a PVD-Standard unit equipped with three dual-source magnetron sputtering sections and power supply systems was employed, as shown in Fig. 3. TORUS-type magnetrons (Kurt Lesker) with 100 mm targets were used, allowing each head to be positioned to match the process zone to the size and geometry of the coated parts. For the deposition of W–Ta–B and W–Ti–B coatings, all magnetrons were equipped with $W_{0.76}Ta_{0.24}B_{2.5}$ and $W_{0.76}Ti_{0.24}B_{2.5}$ targets, respectively [45]. The coated components were placed on a rotating table aligned with the main axis of the process chamber. The deposition parameters for W–Ta–B and W–Ti–B coatings are presented in Table 2.

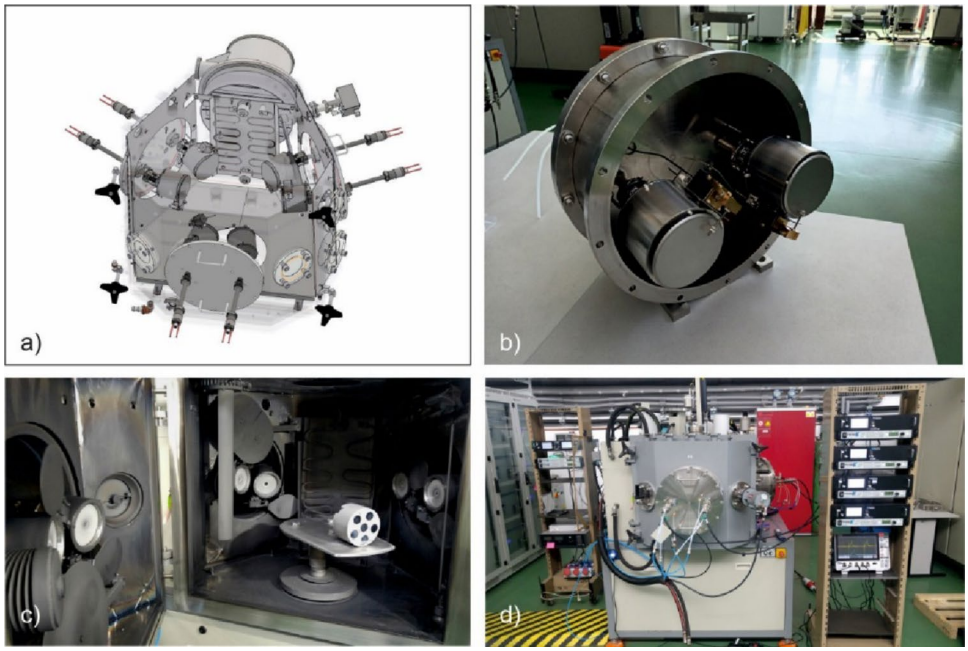

Fig. 3 PVD-Standard unit: **a** 3D model of the process chamber, **b** dual-magnetron plasma source section, **c** interior view of the chamber, **d** overall view of the unit

Table 2 Deposition parameters of W–Ta–B and W–Ti–B coatings deposited by High Power Impulse Magnetron Sputtering (HiPIMS)

Coating	W-Ta-B	W-Ti-B
Target	$W_{0.76}Ta_{0.24}B_{2.5}$	$W_{0.76}Ti_{0.24}B_{2.5}$
Atmosphere	Ar 100%	Ar 100%
Pressure [p]	0.6 Pa	0.6 Pa
Frequency [f]	1000 Hz	1000 Hz
Pulse length [t_p]	20 µs	20 µs
Peak current [I_{peak}]	20 A	20 A
Bias voltage [U_b]	–100 V	–100 V
Time [t]	90 min	90 min
Temperature [T]	450 °C	350 °C

The forging die components inside the process chamber during glow-discharge nitriding and PVD deposition are shown in Fig. 4. Because of significant differences in the mass and geometry of dies and punches, their surface treatments were carried out separately.

2.2.2 Service tests

First, tribological wear tests were conducted using the RTec tribotester. Sample preparation and the entire ball-on-disk test procedure were conducted according to ASTM G99-17 standard. Ball-on-disk tests performed on MFT-5000 tribometer according to ASTM G99-17: alumina ball (Ø6 mm), load 5 N, sliding distance 250 m at 0.2 m/s, room temperature.

Service tests of the coated tools were performed under industrial conditions during the forging of CW724R lead-free alloy elbows. The tests were carried out at an automated production station with graphite-based lubrication, and one tool set was used for each coating variant as part of pilot trials. In this process, the tools were preheated to 250 °C with gas burners, while the billets were heated to an initial temperature of 750 °C. The process was carried out in an automated cycle at a rate of 15 cycles per minute.

The tools were made of ORVAR Supreme steel, heat-treated to 48–50 HRC, and additionally gas-nitrided. Fig. 5 shows the tools mounted on the press and a drawing of the lower die selected for testing.

 https://doi.org/10.1007/s43452-026-01546-x

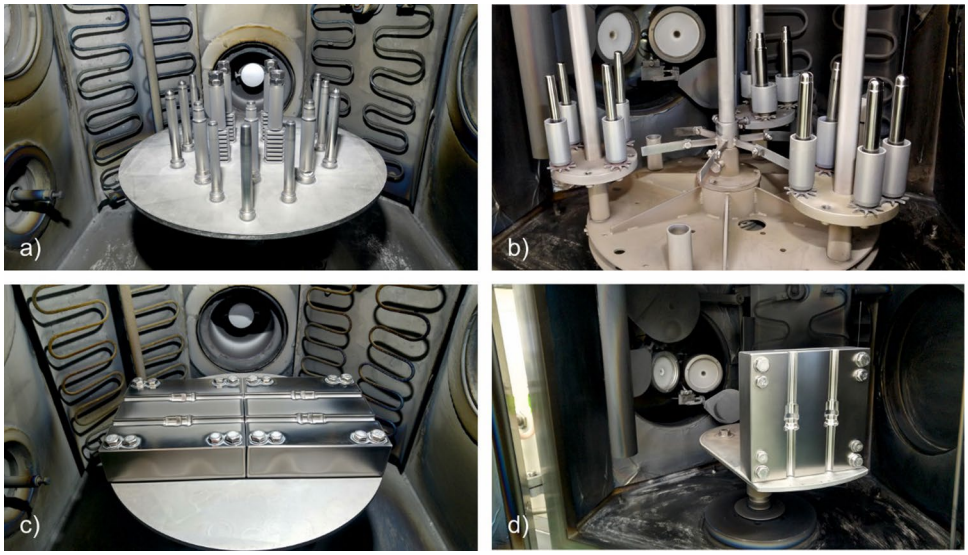

Fig. 4 Forging die components inside the PVD-Standard chamber: **a** glow-discharge nitriding – punches, **b** PVD deposition – punches, **c** glow-discharge nitriding – dies, **d** PVD deposition – dies

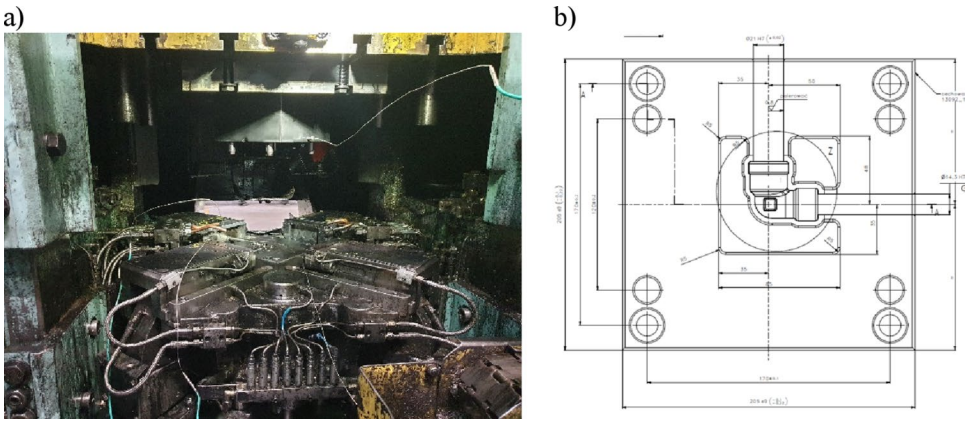

Fig. 5 **a** Tools mounted on the press with thermocouples, **b** drawing of the lower die

As part of the study, process conditions were determined, including tool temperature measurements using a thermocouple placed in a specially prepared hole located approximately 4 mm beneath the working surface. The tool temperature was found to stabilize at approximately 300 °C.

As a reference, tests were first carried out on conventionally used tools. Subsequently, tests were conducted on tools with different WBx-based coating variants. The purpose of these tests was to evaluate how different coating compositions affect tool durability and wear resistance. After completing the service tests, the tools were subjected to detailed analysis. Tool wear was assessed by 3D scanning, which enabled precise evaluation of dimensional changes on the working surface.

3 Results and discussion

3.1 Results of the laboratory studies

For protective coatings intended to resist wear, a number of criteria must be fulfilled. Among these are low surface roughness, a dense and defect-free structure, high hardness, resistance to cracking, and, in the case of applications at elevated temperatures, good thermal stability. Fig. 6 shows the results of roughness and thickness measurements of the deposited films. Both coatings exhibit very low roughness (Fig. 6a, c).

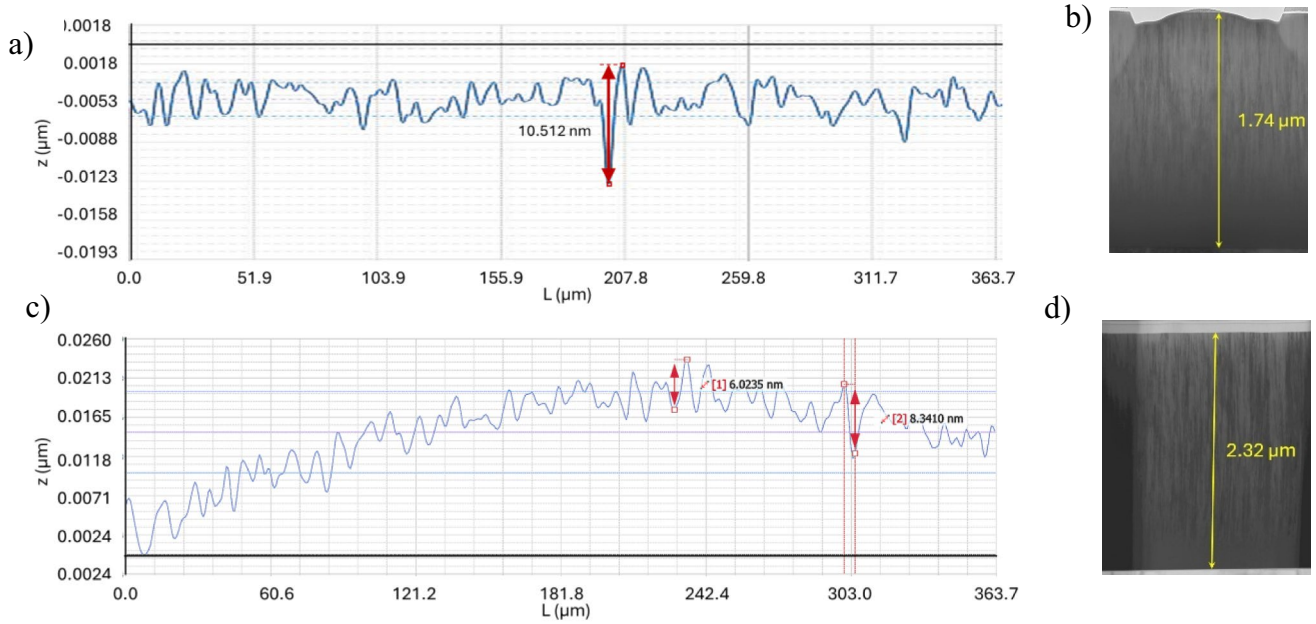

Fig. 6 Roughness and thickness of the deposited coatings: **a** surface profile and **b** TEM image of cross-section of the W–Ti–B film, **c** surface profile and **d** TEM image of cross-section of the W–Ta–B film

For coatings of WB_2 alloyed with tantalum, the roughness is below 10 nm, primarily due to the shape and size of the surface grains. The titanium-doped layer shows a roughness higher by about 20%. SEM images of both coatings are shown in Fig. 6a, d. The surface grains are nearly circular, whereas in the cross-section they appear elongated and aligned perpendicular to the substrate (Fig. 6b, d). The distance *d* measured in TEM images is approximately 50–70 nm and corresponds to the diameter of exemplary columns. TEM studies also reveal the homogeneity of the samples and the absence of visible porosity. In both cases, variations in contrast between individual grains can be observed (Fig. 6b, e), which is characteristic of transition metal borides and indicates the columnar structure of the layer. Such films typically consist of columns composed of a core surrounded by a boundary layer of boron or metal [46, 47]. Additionally, the columns are built from fibers with diameters of approximately 4–7 nm (inset of Fig. 6e). Mayrhofer et al. [46] for example, showed based on HR-TEM observations that columns in magnetron-deposited TiB_2 films with over-stoichiometric boron consist of bundles of coherent ~ 5 nm TiB_2 subcolumns, separated by a 1–2 monolayer-thick B-rich tissue phase with strong covalent bonding. This phenomenon is more pronounced in W–Ta–B layers (Fig. 7e), for which TOF-ERDA measurements (Table 3) indicated a slightly over-stoichiometric boron content, B/(W + Ta) = 2.35. In contrast, for W–Ti–B layers with lower boron content, the boundary tissue phase shifts from B-rich to metal-rich [47]. As a result, the coatings become more flexible.

The reflections in the SAED patterns (Fig. 7c, f) from films grown under Ti- and Ta-ion bombardment exhibit a pronounced 0001 fiber texture with a progressively stronger preferred orientation, consistent with the XRD results (Fig. 3). The primary positions of the diffraction peaks are characteristic of the metastable α-WB_2 phase (P_6/mmm). The shifts toward smaller angles may result from the larger atomic radii of titanium and tantalum (rTa = rTi = 1.46 Å; rW = 1.39 Å) [48]. All spectra are broadened, which, in agreement with the TEM images, confirms the fine-grained structure of the films (fiber diameters; Fig. 7b, e).

Fig. 8 also presents the XRD patterns of samples that, after deposition, were annealed in air at temperatures between 400 and 700 °C. For tantalum-containing films, phase stability can be observed up to nearly 700 °C. However, the spectrum recorded at this temperature also shows peaks corresponding to both boron and tungsten oxides. For boron oxide, the spectrum is characteristic of B_2O_3, which has the highest negative formation energy

 https://doi.org/10.1007/s43452-026-01546-x

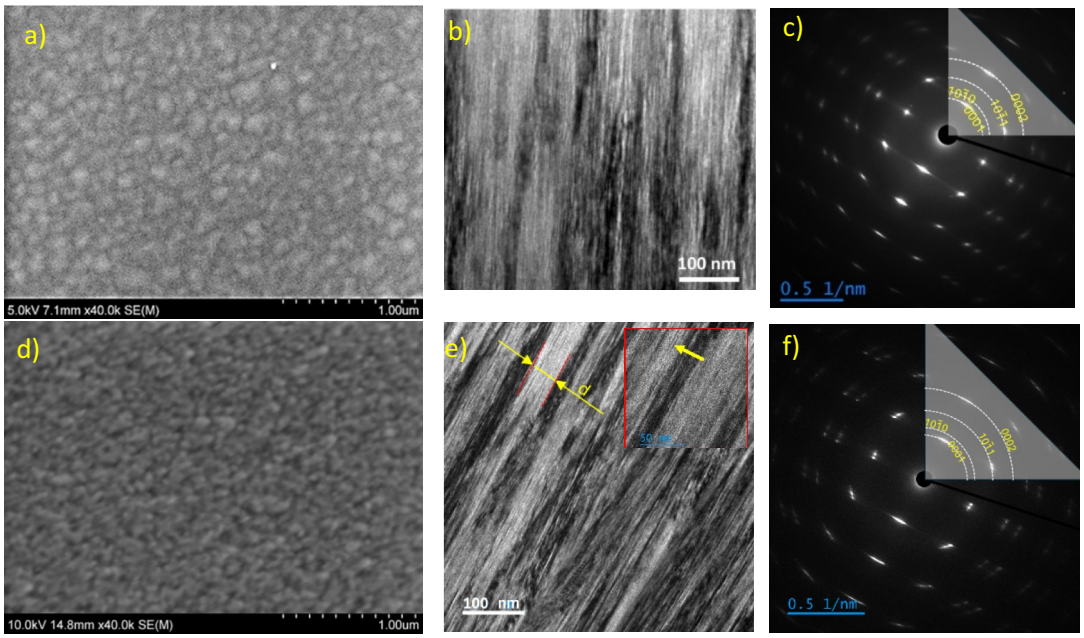

Fig. 7 Microstructural observations: **a** surface morphology (SEM), **b** film cross-section (TEM), and **c** SAED pattern of the W–Ti–B coating, **d** surface morphology, **e** film cross-section, and **f** SAED pattern of the W–Ta–B coating

Table 3 Chemical composition of the deposited films measured using the TOF-ERDA method

	H at%	B at%	C at%	*N*at%	O at%	Ta at%	Ar at%	Ti at%	W at%
W-Ti-B	0.12±0.07	67±5	1.9±0.4	0.3±0.1	<0.1	<0.1	0.3±0.1	6.8±0.7	23±1
W-Ta-B	0.14±0.08	68±5	1.5±0.4	0.1±0.3	0.5±0.2	6.9±0.8	0.4±0.3	<0.1	22±1

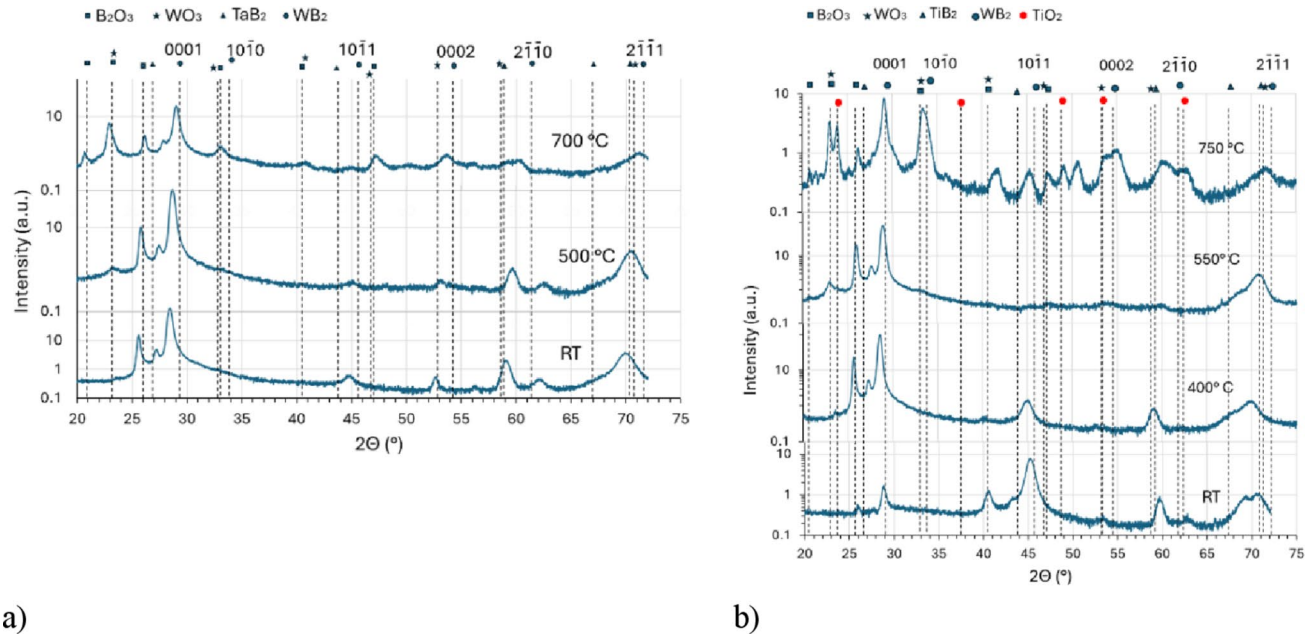

Fig. 8 XRD spectra of **a** W–Ta–B films as deposited (RT) and after annealing in air at 500 and 700 °C, **b** W–Ti–B films as deposited (RT) and after annealing in air at 400, 550, and 700 °C

(–2.562 eV/atom) and crystallizes in the trigonal system. For titanium alloying, annealing causes changes in the intensity of individual α-WB_2 peaks, and already at T_{anne} = 400 °C the recorded crystal structure resembles that of the tantalum-doped case. At 400 °C, a peak appears at 2Θ = 23.8°, characteristic of titanium oxide (rutile TiO_2, tetragonal crystal system). This oxide forms at lower temperatures due to its significantly higher negative formation energy (–3.322 eV/atom) compared with B_2O_3 or WO_3 (–2.188 eV/atom). At 700 °C, the intensity of all oxide peaks increases, indicating coating degradation. This observation is confirmed by SEM surface examinations (Fig. 9)

For the tantalum-alloyed layer, the surface shows no significant changes even after annealing at 500 °C. The situation differs for titanium, where the surface already becomes rougher at 400 °C due to titanium oxide formation. At higher annealing temperatures, i.e., 550 °C, cracks appeared in both coatings. This is attributed to thermal stresses and differences in the thermal expansion of nitrided steel and boride coatings. At 550 °C, titanium-doped coatings show distinct bright spots, while tantalum coatings become less smooth. After annealing at 700 °C, large B_2O_3 grains with a distinct trigonal structure are formed in these areas. In contrast, titanium-alloyed layers form a uniform oxide layer. As shown in Fig. 15, after heating to 700 °C in air, both coatings fail due to cracking and delamination.

As previously noted in the discussion of coating microstructure, metal borides exhibit very high hardness due to their atomic structure, particularly the strong covalent bonds between boron atoms. However, because of boron deficiency in the deposited films, the rigid columnar coatings are enriched with metallic elements [47], leading to increased elasticity but reduced hardness. When the alloying element content is high, bond type is also influenced by electronegativity. Lower electronegativity values [48] for B and Ta or Ti (χTi = 1.54, χTa = 1.50) compared with W (χW = 2.36) lead to different mixtures of ionic, metallic, and covalent bonding. As shown in Table 2, the deposited coatings exhibit different behavior. The increase in elasticity does not result in a loss of hardness. For titanium-alloyed films, nanoindentation measurements show hardness values above 40 GPa, classifying these layers as superhard. For tantalum, the hardness is slightly lower, at 37.8 GPa. At the same time, the reduced Young's modulus values of 380.1 and 359.5 GPa, respectively, yield a high plasticity index (H/E^*) and resistance to plastic deformation (H^3/E^2). Such high hardness can be attributed primarily to solid-solution hardening. In both cases, the titanium and tantalum contents exceed the solubility limit in WB_2, which can lead to supersaturation and the formation of secondary phases, i.e., titanium boride TiB_2 and tantalum boride Table 2. This is confirmed by XRD results, where the α-WB_2 peaks are shifted toward positions corresponding to the above-mentioned borides. Additionally, the relatively small fiber width, ~4–7 nm, contributes to film hardness via the Hall–Petch effect [49, 50]. In addition to increased hardness, W–Ti–B and W–Ta–B coatings also show enhanced toughness, as shown in Table 4. K1c values are 3.7 [35] and 3.4 MPa√m [51], exceeding those measured for commonly used

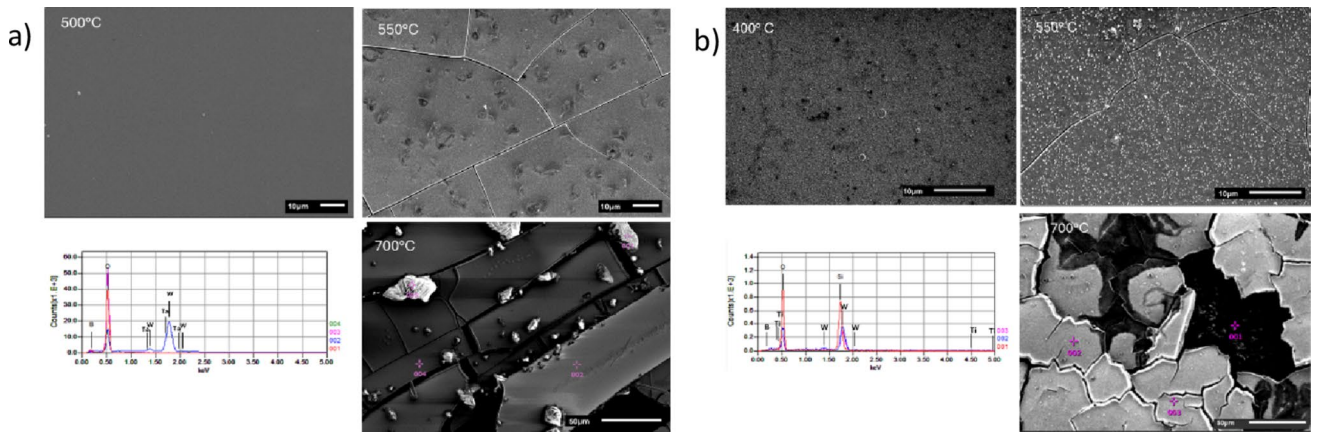

Fig. 9 SEM surface images of samples annealed at 500, 550, and 700 °C with W–Ta–B coatings (**a**), and at 400, 550, and 700 °C with W–Ti–B films. EDS spectra show the chemical composition at selected points of samples annealed at 700 °C

Table 4 Mechanical properties of deposited films: hardness, reduced Young's modulus, plasticity index, resistance to plastic deformation, residual stress, fracture toughness, and Poisson's ratio

	Hardness	Reduced Young's modulus	Plasticity index	Resistance to plastic deformation	Residual stress	Fracture toughness	Poisson's ratio
	H (GPa)	E^* (GPa)	H/E^*	H^3/E^2 (GPa)	σ (GPa)	K_{1C} (MPa√m)	ν
W–Ti–B	40.5 ± 4.6	380.1 ± 49.2	0.117	0.609	−1.01 ± 0.09 [35]	3.7 ± 0.1 [35]	0.27 [40]
W–Ta–B	37.6 ± 2.3	359.5 ± 35.1	0.105	0.411	−1.13 ± 0.10 [50]	3.4 ± 0.3 [50]	–

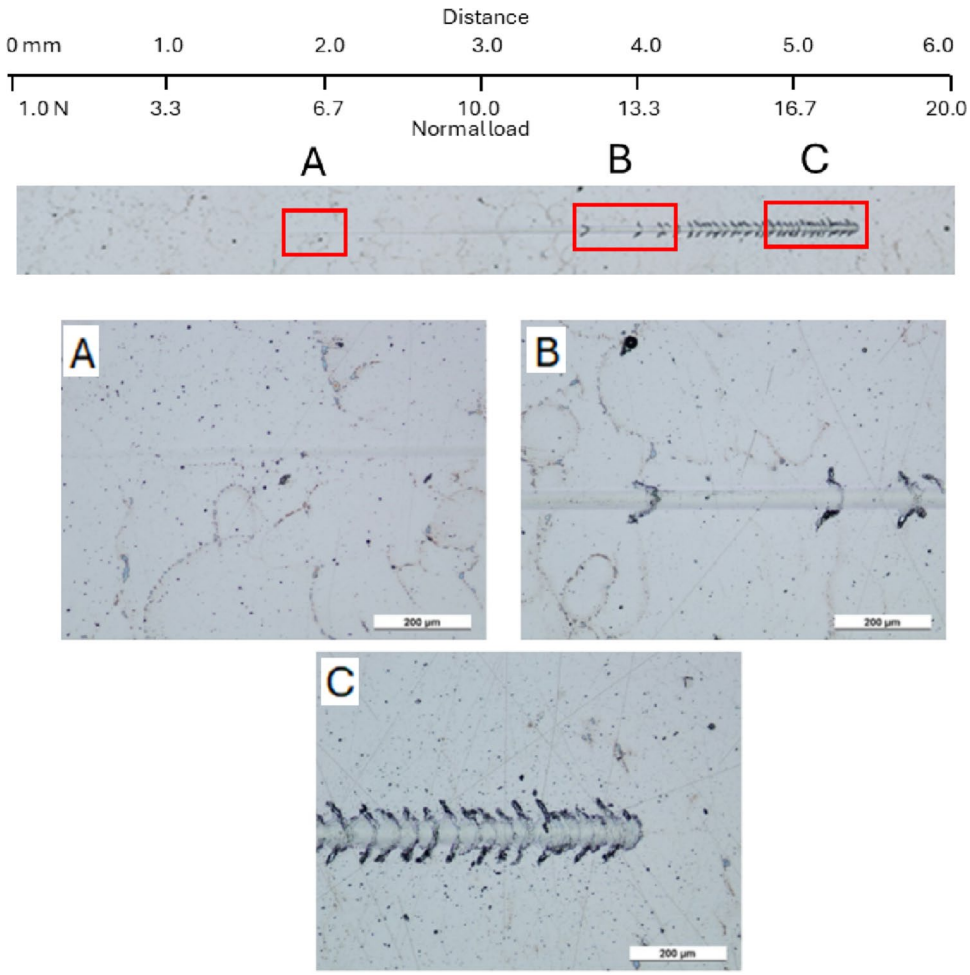

Fig. 10 Scratch morphology after the scratch test for the W–Ti–B coating, with detailed views

titanium nitride protective coatings [51]. The intrinsic compressive stress of both coatings is relatively high and is associated with a high trapped Ar concentration of ~ 0.4 at% (Table 3) [47]. As the Ta or Ti ion flux increases with the HiPIMS method, metal-rich column boundaries are formed and the average column size decreases, causing stress to rise to ~1.01 GPa for titanium [35] and ~1.13 GPa [51] for tantalum, primarily due to residual ion-induced lattice defects.

As shown above, the HiPIMS method enables the formation of a dense structure without observable porosity, achieved through the increased mobility of adatoms resulting from the higher energy of the deposited material's ions compared with the working gas (Ar). Surface diffusion can also contribute to the improved adhesion of the coatings. Figures 10 and 11 present the evolution of surface area during the scratch test with a linearly increasing

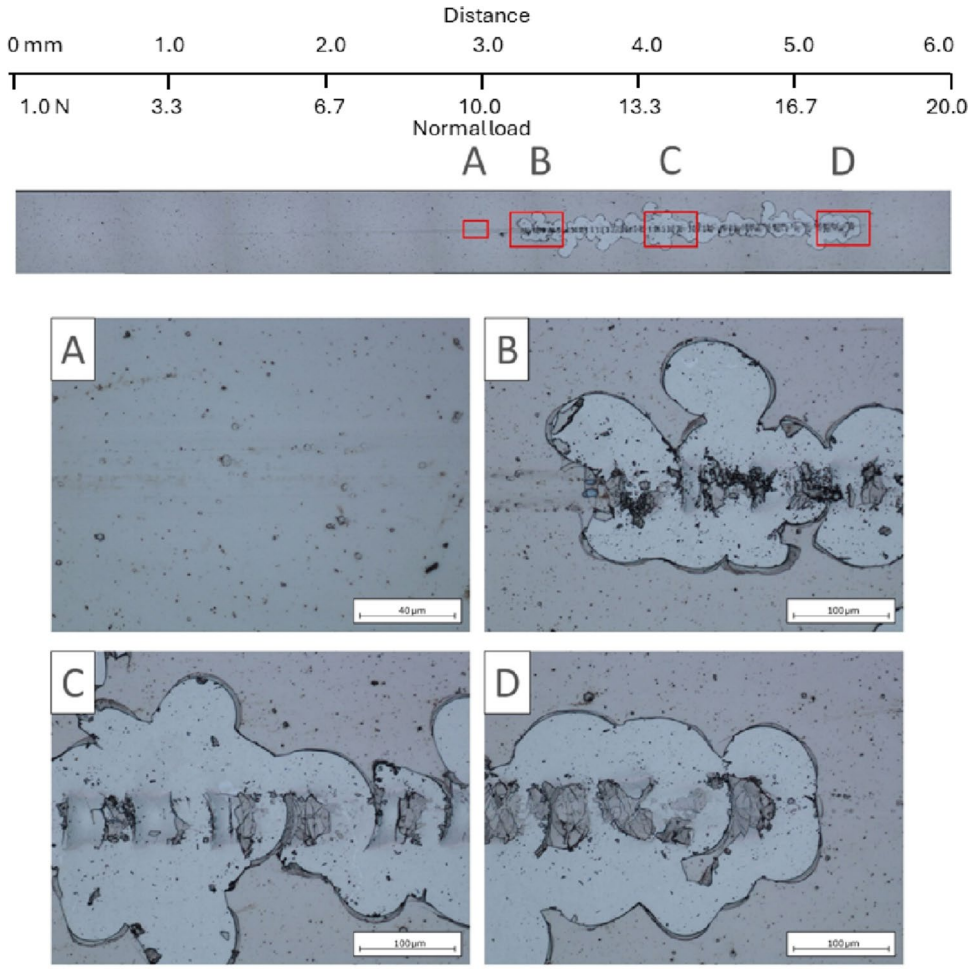

Fig. 11 Scratch morphology after the scratch test for the W–Ta–B coating, with detailed views

load from 1 N to 20 N for W–Ti–B and W–Ta–B coatings, respectively, using a diamond indenter with a rounding radius of 0.2 mm.

The images below the graphs show the detailed appearance of scratches after the scratch test for both coatings. The W–Ti–B coatings exhibit significantly better adhesion to the substrate, with no delamination or chipping observed in the 1–20 N load range; wear occurs mainly by abrasion. The first transverse cracks in the coating appear at a force of L_{c1} = 12.2 N (Fig. 10b). With increasing load, the cracks become denser (Fig. 10c), indicating coating brittleness, although this does not affect adhesion to the substrate. In the case of the W–Ta–B coating, during the initial phase of the test, the coating exhibits a much lower degree of surface development, with no acoustic emission spikes observed in this region. In this load range, coating wear is predominantly abrasive (Fig. 11a). After exceeding 11.3 N, the coating undergoes complete delamination (Fig. 11b). With further load increase, small, detached coating fragments with numerous transverse cracks appear along the wear track (Fig. 11c, d). This mechanism indicates the transfer of tangential stresses through the layer to regions ahead of the indenter, resulting in coating delamination due to shear stresses. This behavior is associated with high cohesion and compressive strength of the coating but limited tensile strength.

Tribological tests also reveal significant differences depending on the coating material. Analysis of the friction coefficient (μ) as a function of the number of cycles shows a typical initial increase, characteristic of the running-in stage (Fig. 12). It should be noted that the W–Ti–B coating exhibited a higher friction coefficient during this stage. For the W–Ta–B coating, the coefficient gradually increased from ~0.2 to over 0.6 after 5000 cycles. In contrast, the W–Ti–B coating reached a stable value of ~0.4 after only 500 cycles, which then remained nearly

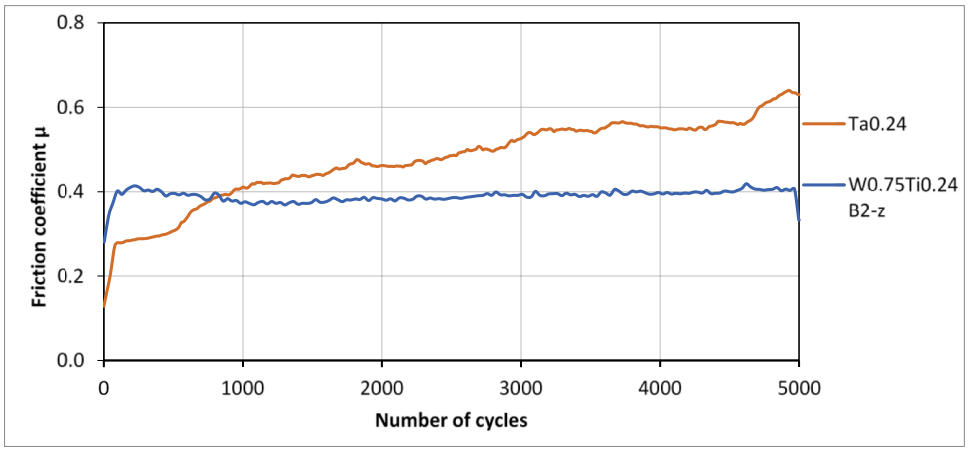

Fig. 12 Evolution of the friction coefficient (μ) as a function of the number of cycles

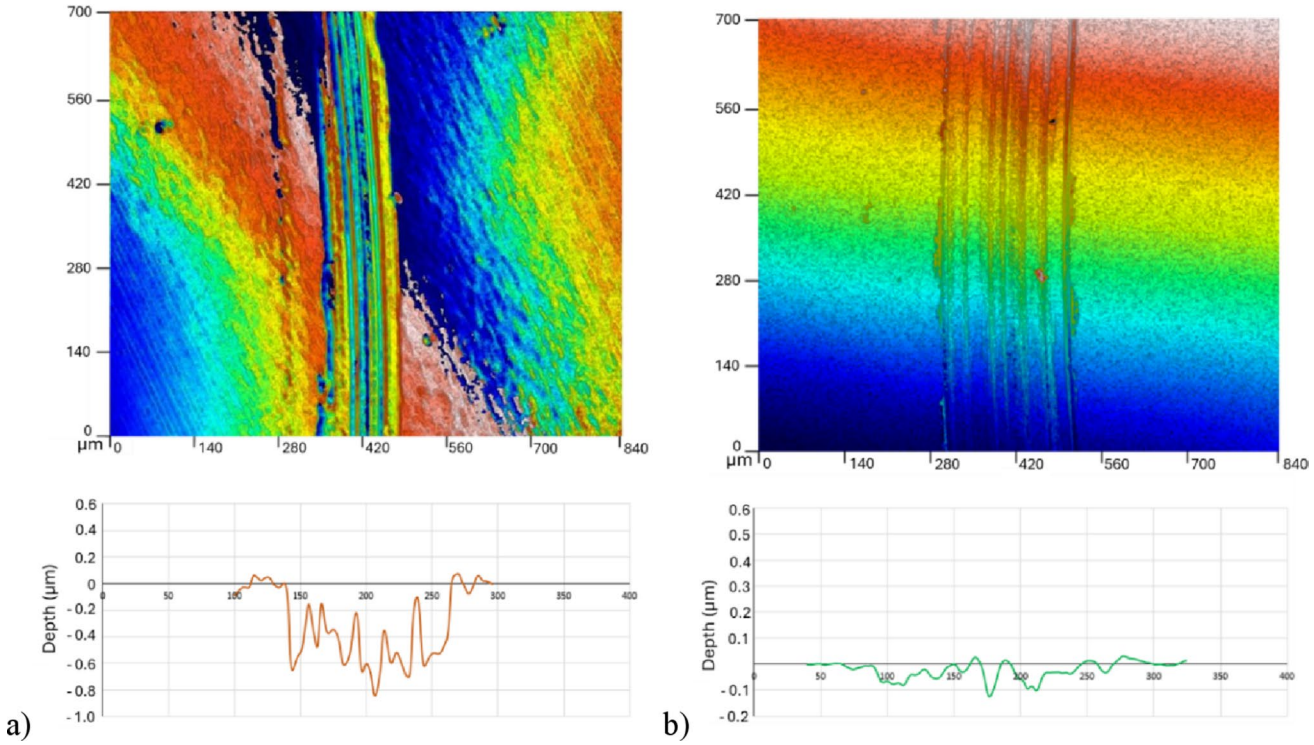

Fig. 13 Surface analysis with wear track profiles: **a** W–Ta–B coating, **b** W–Ti–B coating after 1000 cycles

unchanged until the end of the test. These results indicate the stable frictional behavior of the W–Ti–B coating and its superior wear resistance compared with W–Ta–B.

Surface analysis of the samples after testing, performed with an optical profilometer, confirmed the differences in wear resistance between the coatings. For the W–Ta–B coating, deep and pronounced scratches resulting from ball interaction were observed (Fig. 13a). In contrast, for the W–Ti–B coating, the wear tracks were shallower and narrower, indicating lower susceptibility to abrasive wear. Both coatings demonstrated wear resistance even without the use of additional lubricants, with the W–Ti–B coating showing distinctly higher resistance (Fig. 13b).

Before applying the tools under industrial conditions, additional tests were conducted to verify whether the properties of the coatings were retained after transferring the deposition process from laboratory to industrial equipment. For this purpose, hardness and adhesion of the coatings were evaluated.

The hybrid layers produced exhibited significantly higher surface hardness compared with nitrided QRO steel. The hardness distribution as a function of depth (h_m) is shown in Fig. 14a. Measurements were performed using a CSM Nano-Hardness Tester with a Berkovich indenter, as a function of indentation depth. Fig 14b, c show the surface of W–Ta–B and W–Ti–B coatings, respectively, after adhesion testing with a Rockwell indenter. In the case of the W–Ta–B coating, only radial cracks were observed, with no local coating spallation. In contrast, the W–Ti–B coating exhibited no visible damage around the indentation. This confirms the significantly lower brittleness of the W–Ti–B coating and its very good adhesion to the substrate. The results of these verification tests are consistent with those obtained during the "laboratory studies" phase.

In summary, laboratory tests of coatings with tantalum addition show lower hardness and resistance to plastic deformation but greater resistance to oxidation at high temperatures and better adhesion. For titanium-based coatings, the obtained films are superhard while maintaining a relatively low Young's modulus. However, during oxidation at 400 °C, surface changes associated with the formation of TiO_2 oxide can be observed. Since the film delaminates almost immediately at the onset of cracking during the scratch test, the oxide formed on the surface may paradoxically have a beneficial effect. Specifically, nanoparticles of this oxide exhibit friction-reducing properties during tribological tests [52].

Because these coatings are very smooth, exhibit very high hardness, and at the same time possess reduced stiffness—which increases resistance to cracking—and remain stable in oxidizing environments even at temperatures up to 500 °C, they are strong candidates for industrial applications.

3.2 Results of the industrial studies

The tools with the new coatings were tested in the hot forging process described above. In Fig. 15, the temperature profile as a function of time is shown for the tool selected for testing. The figure clearly shows a rapid increase in temperature to 220 °C during the first 200 s of forging, resulting from the intense heating of the tool by the hot billet material. Subsequently, the temperature gradually stabilizes, reaching approximately 300 °C.

For comparison, nitrided tools were also tested as a reference to the previously applied technology. The table below presents the numerical results of tool life, expressed as the number of forgings produced with a single tool.

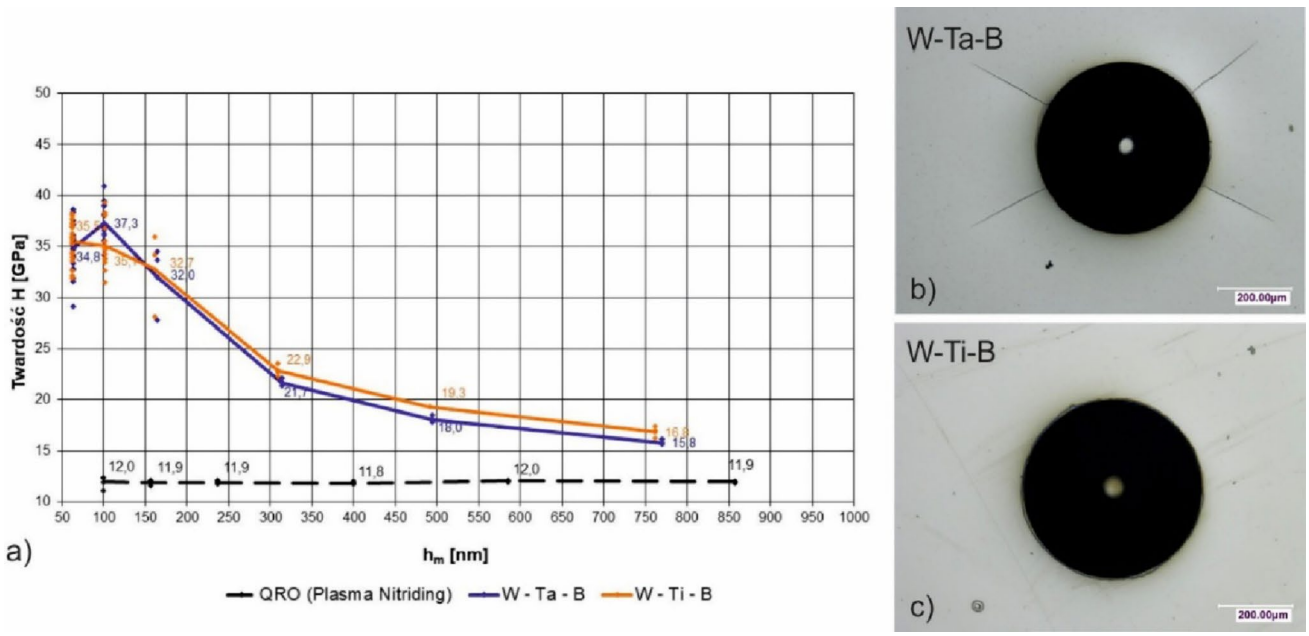

Fig. 14 Hardness distribution results for hybrid "nitriding layer/PVD coating" systems: **a** hardness distribution of the hybrid layers: "nitriding layer + W–Ta–B coating" and "nitriding layer + W–Ti–B coating", **b**, **c** indentation views

 https://doi.org/10.1007/s43452-026-01546-x

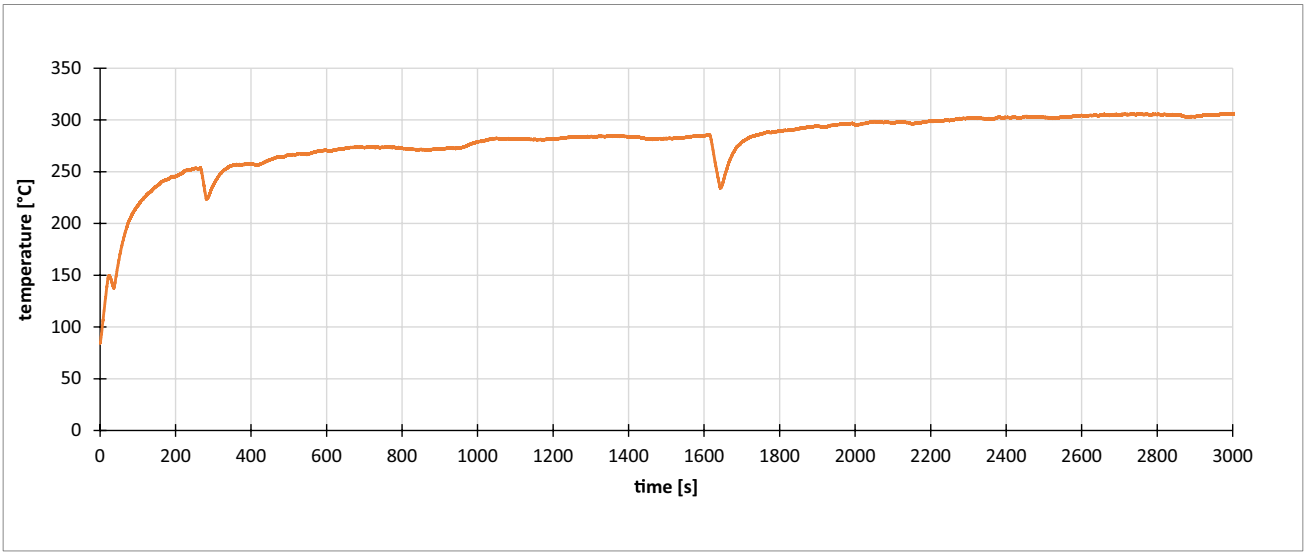

Fig. 15 Temperature of the lower die measured 4 mm below the surface using a thermocouple

Table 5 Service life of tools tested in the forging process

No.	Surface treatment	Tool life [number of forgings]
1	Nitriding	62,388
2	Nitriding + W–Ta–B coating	109,151
3	Nitriding + W–Ti–B coating	113,316

For comparison, nitrided tools were also tested as a reference to the previously applied technology. The results presented in Table 5; Fig. 16 stem from pilot industrial trials using one tool set per surface treatment variant (nitriding only, nitriding + W-Ta-B, nitriding + W-Ti-B). These development tests, spanning approximately 8–12 months, measured tool life as the exact number of forgings produced until the wear criterion (> 0.3 mm flank wear) was reached. Replicates were not performed due to production constraints, including low order volumes and short series of ~ 10–15 thousand pieces every 2–3 months, which would require several years to repeat fully. Despite this, the trials demonstrated consistent performance and lifetime improvements of 75–80% for the coated variants relative to nitriding alone. No significant scatter was observed, as each trial followed identical process conditions.

The results presented in Table 5 demonstrate a significant improvement in tool life with both coatings, corresponding to an increase of approximately 75% for W–Ta–B and 80% for W–Ti–B.

For a quantitative assessment of tool wear before and after forging, the tools were scanned, and the results before and after service were compared. The results of this comparison are shown in Fig. 16.

The results of this comparison indicate the occurrence of wear on the surface in key areas – along the edges near the die bridge, where the forging material flows out, and in the center of the die cavity. The die qualifies for replacement when maximum wear depth exceeds 0.3 mm, per the forging facility's industrial standard for this process. This threshold aligns with dimensional tolerances ($\pm$ 0.2 mm on critical features) and ensuring geometric conformity.

In Fig. 16a, the die nitrided after 62,388 forgings was withdrawn from service due to wear in the lower part. Similarly, in Fig. 16b, wear exceeding 0.3 mm can be observed on the nitrided + W–Ta–B coated die, which led to its withdrawal after a significantly longer service life of 109,151 forging cycles. The next die (nitrided + W–Ti–B coating), shown in Fig. 16c, has not yet completed its full service life, since after 113,316 forgings its wear was relatively the smallest compared to the others. These observations demonstrated that the W–Ti–B coating

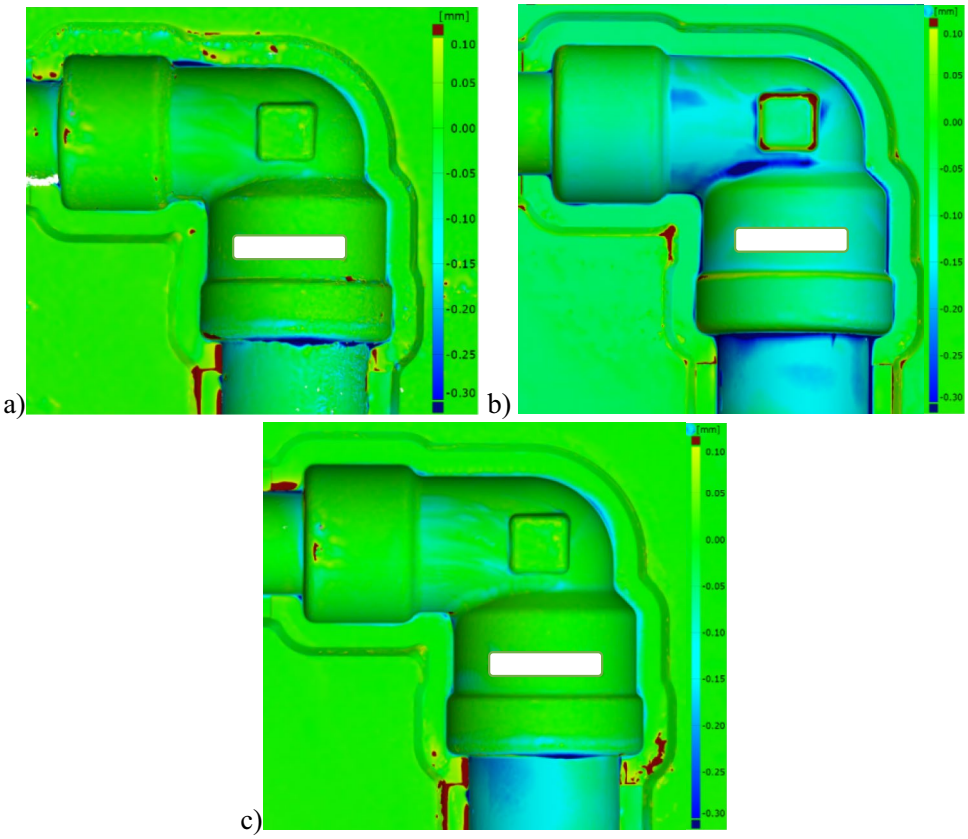

Fig. 16 Surface scan deviation results for tools before and after forging: **a** nitrided after 62,388 forgings, **b** nitrided + W–Ta–B coating after 109,151 forgings, **c** nitrided + W–Ti–B coating after 113,316 forgings

provides the highest wear resistance, which is consistent with the earlier results of the scratch adhesion tests (Figs. 10 and 11) and the abrasive wear resistance tests shown in Fig. 13.

Post-service wear was primarily assessed via macro-observations and non-destructive 3D scanning to quantify flank wear depth (> 0.3 mm criterion) and volumetric loss. Detailed SEM/EDS examinations of worn surfaces, including tribochemical aspects such as oxide layers and workpiece material transfer (CW724R alloy), await complete tool exhaustion and production withdrawal (several additional months), as timeline extensions were not possible. These advanced analyses are planned for future work to provide deeper mechanistic insights.

4 Summary and conclusions

This study demonstrates the successful development and validation of advanced hybrid surface treatments for hot forging tools using W–Ti–B and W–Ta–B nanocomposite coatings deposited by High Power Impulse Magnetron Sputtering (HiPIMS). The study covers the entire cycle from "concept to implementation." The research begins with basic laboratory testing of the innovative material. Next, protective coatings are applied to plasma-nitrided forging dies on an industrial scale, which are then successfully operated on the production line. The coatings exhibit excellent mechanical and thermal properties, including high hardness, improved elasticity, good adhesion, and oxidation resistance up to 500 °C. Laboratory investigations revealed that the W–Ti–B coating provides superior properties relevant to tool performance. In particular:

- Regardless of the alloying element, both films are crystalline and display a distinct columnar structure. Furthermore, the deposited samples exhibit a low surface roughness of about 10 nm.

- The higher plasticity index H/E (0.117 for Ti and 0.105 for Ta) and resistance to plastic deformation H^3/E^2 (0.61 for Ti and 0.41 for Ta) of the W–Ti–B layers contribute to greater fracture toughness (K_{1c}), while also qualifying as superhard.
- The adhesion of films without an additional stress-compensating interlayer is similar in both cases (L_{c1} at 12.2 N for Ti and 11.3 N for Ta). However, different film failure mechanisms were observed during testing. For tantalum-containing layers, delamination and chipping were observed, whereas for titanium, wear occurred mainly through an abrasive mechanism. This difference is related to the lower deposition temperature of Ta-containing films, which results in inferior mechanical properties.
- The nearly constant coefficient of friction, despite the lower oxidation resistance of W–Ti–B, positively contributes to extended surface service life and reduces wear, as the oxide layer formed at elevated temperatures can act as a solid lubricant.
- The above-mentioned properties of titanium-containing coatings improve the wear resistance of the tested layers deposited on forging tools.

Industrial trials confirmed that both coating systems significantly extend tool life by approximately 75% for W–Ta–B and over 80% for W–Ti–B compared to conventional nitrided tools, reducing per-part tooling costs by ~40% and tool change downtime by 5–10% while recovering coating investment within 3–6 months of production. These results validate their suitability for demanding hot forging applications, demonstrate economic viability for industrial scale-up, and highlight their potential for broader implementation across metal forming sectors.

These results validate their suitability for demanding hot forging applications including lead-free bronzes (CW724R) and ferrous alloys, highlighting their potential for broader implementation across metal forming sectors due to equivalent tool operating conditions (contact pressures > 1000 MPa, dry sliding friction, tool temperatures ~ 400 °C) [53].

Acknowledgements We acknowledge support from the National Center for Research and Development via the TECHMATSTRATEG program grant no. TECHMATSTRATEGIII/0017/2019, from the European Union Horizon 2020 research and innovation program under NOMATEN Teaming grant (agreement no. 857470) and from the European Regional Development Fund via the Foundation for Polish Science International Research Agenda PLUS program grant No. MAB PLUS/2018/8. The National Science Centre (NCN, Poland) 2022/47/BST8/01296 supported in TOF ERDA chemical composition measurement and scratch tests were made on aparatus funded by this project.

Data availability Data will be made available on reasonable request.

Declarations

Conflict of interest The authors declare that they have no known competing financial interests or personal relationships that could have appeared to influence the work reported in this paper. On behalf of all authors, the corresponding author states that there is no conflict of interest.

References

1. Gronostajski Z, Kaszuba M, Hawryluk M, Zwierzchowski M. A review of the degradation mechanisms of the hot forging tools. Archives Civil Mech Eng. 2014;14:528–39. https://doi.org/10.1016/j.acme.2014.07.002.

2. Widomski P, Gronostajski Z. Comprehensive review of methods for increasing the durability of hot forging tools. Procedia Manuf. 2020;47:349–55. https://doi.org/10.1016/j.promfg.2020.04.280.
3. Smolik J. Hard protective layers on forging dies—development and applications. Coatings. 2021. https://doi.org/10.3390/coatings11040376.
4. Rakhadilov B, Shynarbek A, Kakimzhanov D, Muktanova N, Kusainov R. Influence of high-speed arc metallization wire feed rate on tribological and corrosion properties of 30HGSA steel coatings. Mater Sci-Poland. 2024;42:171–80. https://doi.org/10.2478/msp-2024-0030.
5. Górnik M, Lachowicz M, Łatka L. Corrosion resistance of PPTA Ni-based hardfacing layers. Mater Science-Poland. 2024;42:66–78. https://doi.org/10.2478/msp-2024-0040.
6. Kannan PR, Thanigaivelan R, Thiraviam R, Pradeep Kumar K. Performance studies on hybrid nano-metal matrix composites for wear and surface quality. Mater Sci-Poland. 2023;41:288–300. https://doi.org/10.2478/msp-2023-0020.
7. Lachowicz MM. Insight into the microstructural stability and thermal fatigue behavior of nitrided layers on martensitic hot forging tools. Mater Science-Poland. 2025;43:1–17. https://doi.org/10.2478/msp-2025-0005.
8. Hawryluk M, Dudkiewicz Ł, Zwierzchowski M, Polak S, Lachowicz M, Ziemba J, et al. Influence of the nitriding process on the durability of tools used in the production of automotive forgings in industrial hot die forging processes on hammers. Mater Sci-Poland. 2024;42:113–30. https://doi.org/10.2478/msp-2024-0047.
9. Dennis JK, Mahmoud EAAG. Wear resistance of surface-treated hot forging dies. Tribol Int. 1987;20:10–7. https://doi.org/10.1016/0301-679X(87)90003-X.
10. Son MJ, Kang SS, Lee EA, Kim KH. Properties of TiBN coating on the tool steels by PECVD and its applications. J Mater Process Technol. 2002;130–131:266–71. https://doi.org/10.1016/S0924-0136(02)00748-3.
11. Behrens BA, Bistron M, Bach FW, Moehwald K, Deisser TA, Denkena B, et al. Manufacturing of reinforced high precision forging dies. Steel Res Int. 2009;80:878–86. https://doi.org/10.2374/SRI09SP130.
12. Paschke H, Stueber M, Ziebert C, Bistron M, Mayrhofer P. Composition, microstructure and mechanical properties of boron containing multilayer coatings for hot forming tools. Surf Coat Technol. 2011;205:S24–8. https://doi.org/10.1016/j.surfcoat.2011.04.097.
13. Behrens BA, Bräuer G, Paschke H, Bistron M. Reduction of wear at hot forging dies by using coating systems containing boron. Prod Eng Res Devel. 2011. https://doi.org/10.1007/s11740-011-0308-z.
14. Höck K, Spies HJ, Larisch B, Leonhardt G, Buecken B. Wear resistance of prenitrided hardcoated steels for tools and machine components. Surf Coat Technol. 1997. https://doi.org/10.1016/S0257-8972(96)02914-3.
15. Munz WD, Smith IJ. Wear resistant PVD coatings for high temperature (950°) applications, in: Proceedings, Annual Technical Conference - Society of Vacuum Coaters, 1999.
16. Smolik J, Walkowicz J, Tacikowski J. Influence of the structure of the composite: nitrided layer/PVD coating on the durability of tools for hot working. Surf Coat Technol. 2000. https://doi.org/10.1016/S0257-8972(99)00593-9.
17. Navinšek B, Panjan P, Gorenjak F. Improvement of hot forging manufacturing with PVD and DUPLEX coatings. Surf Coat Technol. 2001;137:255–64. https://doi.org/10.1016/S0257-8972(00)01115-4.
18. Walkowicz J, Smolik J, Tacikowski J. Modern plasma technologies for anti-wear applications. High Temperature Material Processes (An International Quarterly of High-Technology Plasma Processes). 2001;5:6. https://doi.org/10.1615/HighTempMatProc.v5.i4.50.
19. Pellizzari M, Molinari A, Straffelini G. Thermal fatigue resistance of plasma duplex-treated tool steel. Surf Coat Technol. 2001;142–144:1109–15. https://doi.org/10.1016/S0257-8972(01)01223-3.
20. Panjan P, Urankar I, Navinšek B, Terčelj M, Turk R, Cekada M, Leskovšek V. Improvement of hot forging tools with duplex treatment. Surf Coat Technol. 2002. https://doi.org/10.1016/S0257-8972(01)01634-6.
21. Dobrzański LA, Polok M, Adamiak M. Structure and properties of wear resistance PVD coatings deposited onto X37CrMoV5-1 type hot work steel. J Mater Process Technol. 2005. https://doi.org/10.1016/j.jmatprotec.2005.02.164.
22. Fumiaki H, Ken I, Inoue KI. Development of novel multi-layer PVD coating for hot forging dies and punches, in: ICPMT2006 - Progress of Machining Technology - Proceedings of the 8th International Conference on Progress of Machining Technology, 2006.
23. Bobzin K, Hirt G, Springorum F, Zitz U, Steinhof F, Bagcivan N, et al. Hot forging of C45 using PVD (Ti,Al)N/γ-Al_2O_3 coated dies. Steel Res Int. 2010. https://doi.org/10.1002/srin.201000031.
24. Tillmann W, Vogli E, Momeni S. Improvement of press dies used for the production of diamond composites by means of DUPLEX-PVD-coatings. Surf Coat Technol. 2010. https://doi.org/10.1016/j.surfcoat.2010.08.048.
25. Ge PL, Bao MD, Zhang HJ, You K, Liu XP. Effect of plasma nitriding on adhesion strength of CrTiAlN coatings on H13 steels by closed field unbalanced magnetron sputter ion plating. Surf Coat Technol. 2013;229:146–50. https://doi.org/10.1016/j.surfcoat.2012.08.002.
26. Demir M, Kanca E, Karahan İH. Effect of saccharin addition on formation, wear and corrosion resistance of electrodeposited Ni-Cr coatings. Mater Sci-Poland. 2023;41:111–25. https://doi.org/10.2478/msp-2023-0036.
27. Chang YY, Amrutwar S. Effect of plasma nitriding pretreatment on the mechanical properties of AlCrSiN-coated tool steels. Materials. 2019. https://doi.org/10.3390/MA12050795.

28. Rao J, Sharma A, Rose T. Titanium aluminium nitride and titanium boride multilayer coatings designed to combat tool wear. Coatings. 2018;8:1–12. https://doi.org/10.3390/coatings8010012.
29. Greczynski G, Petrov I, Greene JE, Hultman L, Paradigm shift in thin-film growth by magnetron sputtering: From gas-ion to metal-ion irradiation of the growing film, Journal of Vacuum ScienceTechnology, Vacuum A. Surfaces, and Films 37 (2019). https://doi.org/10.1116/1.5121226
30. Bartosik M, Rumeau C, Hahn R, Zhang ZL, Mayrhofer PH. Fracture toughness and structural evolution in the TiAlN system upon annealing. Sci Rep. 2017;7:16476. https://doi.org/10.1038/s41598-017-16751-1.
31. Wicher B, Pshyk OV, Li X, Bakhit B, Rogoz V, Petrov I, et al. Superhard oxidation-resistant $Ti_{1-x}Al_xB_y$ thin films grown by hybrid HiPIMS/DCMS co-sputtering diboride targets without external substrate heating. Mater Des. 2024;238:112727. https://doi.org/10.1016/j.matdes.2024.112727.
32. Mościcki T, Psiuk R, Radziejewska J, Wiśniewska M, Garbiec D. Properties of Spark Plasma Sintered compacts and Magnetron Sputtered coatings made from Cr, Mo, Re and Zr alloyed Tungsten Diboride. Coatings. 2021;11:1378. https://doi.org/10.3390/coatings11111378.
33. Xia R, Zhang K, Shu F, Zhang X, Yan L, Li C. Effects of B content on wear and corrosion resistance of laser-cladded Co-based alloy coatings. Mater Sci-Poland. 2023;41:13–23. https://doi.org/10.2478/msp-2023-0040.
34. Fuger C, Schwartz B, Wojcik T, Moraes V, Weiss M, Limbeck A, et al. Influence of Ta on the oxidation resistance of WB2−z coatings. J Alloys Compd. 2021;864:158121. https://doi.org/10.1016/j.jallcom.2020.158121.
35. Mościcki T, Psiuk R, Jarząbek D, Ciemiorek-Bartkowska M, Kulikowski K, Jasiński J, et al. Effect of titanium and deposition parameters on microstructure and mechanical properties of W-Ti-B thin films deposited by high power impulse magnetron sputtering. Surf Coat Technol. 2024. https://doi.org/10.1016/j.surfcoat.2024.130915.
36. Musil J. Hard and superhard nanocomposite coatings. Surf Coat Technol. 2000;125:322–30. https://doi.org/10.1016/S0257-8972(99)00586-1.
37. Hahn R, Moraes V, Limbeck A, Polcik P, Mayrhofer PH, Euchner H. Electron-configuration stabilized (W,Al)B2 solid solutions. Acta Mater. 2019;174:398–405. https://doi.org/10.1016/j.actamat.2019.05.056.
38. Chen Z, Huang Y, Koutná N, Gao Z, Sangiovanni DG, Fellner S, et al. Large mechanical properties enhancement in ceramics through vacancy-mediated unit cell disturbance. Nat Commun. 2023;14:8387. https://doi.org/10.1038/s41467-023-44060-x.
39. Moraes V, Riedl H, Fuger C, Polcik P, Bolvardi H, Holec D, et al. Ab initio inspired design of ternary boride thin films. Sci Rep. 2018;8:9288. https://doi.org/10.1038/s41598-018-27426-w.
40. Maździarz M, Psiuk R, Krawczyńska A, Lewandowska M, Mościcki T. Effect of Zirconium doping on the mechanical properties of W<sub-script>1-x</sub-script>Zr<sub-script>x</sub-script>B<sub-script>2</sub-script> on the basis of first-principles calculations and magnetron sputtered films. Arch Civ Mech Eng. 2022;22:193. https://doi.org/10.1007/s43452-022-00513-6.
41. Li X, Bakhit B, Jõesaar MPJ, Hultman L, Petrov I, Greczynski G. Toward energy-efficient physical vapor deposition: routes for replacing substrate heating during magnetron sputter deposition by employing metal ion irradiation. Surf Coat Technol. 2021;415:127120. https://doi.org/10.1016/j.surfcoat.2021.127120.
42. Psiuk R, Mościcki T, Chrzanowska-Giżyńska J, Kurpaska Ł, Radziejewska J, Denis P, et al. Mechanical and thermal properties of W-Ta-B coatings deposited by high-power impulse magnetron sputtering (HiPIMS). Materials. 2023. https://doi.org/10.3390/ma16020664.
43. Psiuk R, Chrzanowska-Giżyńska J, Denis P, Wyszkowska E, Wiśniewska M, Lipińska M, et al. Microstructural and properties investigations of tantalum-doped tungsten diboride ceramic coatings via HiPIMS and RF magnetron sputtering. Arch Civ Mech Eng. 2024;24:239. https://doi.org/10.1007/s43452-024-01050-0.
44. Oliver WC, Pharr GM. Measurement of hardness and elastic modulus by instrumented indentation: advances in understanding and refinements to methodology. J Mater Res. 2004;19:3–20. https://doi.org/10.1557/jmr.2004.19.1.3.
45. Garbiec D, Wiśniewska M, Marczewski M, Mościcki T, Psiuk R, Chrzanowska-Giżyńska J, Krawczyńska A, Adamczyk-Cieślak B, Lewandowska M. Spark Plasma Sintering Of Tungsten Boride With Transition Metals Admixture, in: World PM 2022 Congress Proceedings, 2022.
46. Mayrhofer PH, Mitterer C, Wen JG, Greene JE, Petrov I. Self-organized nanocolumnar structure in superhard TiB2 thin films. Appl Phys Lett. 2005. https://doi.org/10.1063/1.1887824.
47. Bakhit B, Engberg DLJ, Lu J, Rosen J, Högberg H, Hultman L, et al. Strategy for simultaneously increasing both hardness and toughness in ZrB2-rich Zr1−xTaxBy thin films. J Vac Sci Technol A. 2019. https://doi.org/10.1116/1.5093170.
48. Magnuson M, Hultman L, Högberg H. Review of transition-metal diboride thin films. Vacuum. 2022;196:110567. https://doi.org/10.1016/j.vacuum.2021.110567.
49. Hall EO. The deformation and ageing of mild steel: III discussion of results. Proc Phys Soc B. 1951;64:747–53. https://doi.org/10.1088/0370-1301/64/9/303.
50. Petch N. The cleavage strength of polycrystals. J Iron Steel Inst. 1953;174:25–8.
51. Fuger C, Moraes V, Hahn R, Bolvardi H, Polcik P, Riedl H, et al. Influence of tantalum on phase stability and mechanical properties of WB2. MRS Commun. 2019;9:375–80. https://doi.org/10.1557/mrc.2019.5.

52. Birleanu C, Pustan M, Cioaza M, Molea A, Popa F, Contiu G. Effect of TiO2 nanoparticles on the tribological properties of lubricating oil: an experimental investigation. Sci Rep. 2022;12:5201. https://doi.org/10.1038/s41598-022-09245-2.
53. Widomski P, Kaszuba M, Barełkowski A, Smolik J, Garbiec D, Ciemiorek-Bartkowska M, et al. WTaB coatings as effective solutions for increasing die durability in lead-free brass alloy flashless hot forging process. Wear. 2025;571:205849. https://doi.org/10.1016/j.wear.2025.205849.

Authors and Affiliations

T. Mościck[1] · Pawel Widomski[2,3] · M. Kaszuba[2,3] · E. Wojtiuk[1] · T. Stasiak[4] · K. Kulikowski[5] · R. Psiuk[1] · M. Wiśniewska[6] · J. Smolik[7]

✉ Pawel Widomski
pawel.widomski@pwr.edu.pl

[1] Institute of Fundamental Technological Research, Polish Academy of Sciences, Pawinskiego 5B, Warsaw 02-106, Poland

[2] Department of Metal Forming, Welding and Metrology Faculty of Mechanical Engineering, Wroclaw University of Science and Technology, Wroclaw 50-370, Poland

[3] Center for Materials Engineering and Metal Forming, Wrocław University of Science and Technology, Wrocław 50-371, Poland

[4] NOMATEN Centre of Excellence National Centre for Nuclear Research, Andrzeja Soltana 7, 05-400 Otwock, Poland

[5] Faculty of Materials Science and Engineering, Warsaw University of Technology, Woloska 141, Warsaw 02-507, Poland

[6] Łukasiewicz Research Network - Poznan Institute of Technology, Estkowskiego 6, Poznan 61-755, Poland

[7] Łukasiewicz Research Network - Institute for Sustainable Technologies, Pulaskiego 6/10, Radom 26-600, Poland